The effect of edge and impurities sites properties on their localized states in semi-infinite zigzag edged 2D honeycomb graphene sheet

Maher Ahmed

Department of Physics and Astronomy,

University of Western Ontario, London ON N6A 3K7, Canada and

Physics Department, Faculty of Science,

Ain Shams University, Abbsai, Cairo, Egypt[*]

Abstract

In this work, the tridiagonal method [1] is used to distinguish between edges modes and area modes to study the edge sites properties effect on edge localized states of semi-infinite zigzag 2D honeycomb graphene sheet. The results show a realistic behavior for the dependance of edge localized states of zigzag graphene on the edge sites properties which explaining the experimental results of measured local density of states at the edge of graphene [2], while at the same time removing the inconsistence between the semi-conductor behavior found in the experimental data for fabricated GNRs [3, 4] and the expected theoretical semi-metallic behavior calculated without considering the edge properties effect on the edge localized states [5–8].

[*] mahmed62@uwo.ca

I. INTRODUCTION

It is known that the 2D materials with zigzag edged nanoribbons of 2D honeycomb lattice structure has peculiar flat localized edge states at the Fermi level [1, 5–8], which is a result of the zigzag geometry effect on the particles hopping flow in its edges sites.

These edge states are known to be important due to their effect on the electronic properties and as a consequence in a variety of future applications of the famous Zigzag Graphene Nanoribbons (ZGNR) [4, 8]. The edge localized states are, in general, dependent upon the ribbon size and purity of the sample [1, 9]. From a theoretical point of view, the edges states depends on the probability for an electron to hop from a site in the edge to a bulk site, or to impurity site in the neighborhood. The edge atoms have a different coordination number from the bulk atoms, this leads to a different hopping parameter between the edge atoms and the bulk one. Such a difference is not usually considered in previous calculations for that ZGNR edge localized states with different approaches [5–8], these calculations show inconsistencies with experimental results for all fabricated GNRs that has semiconductor behavior [3, 4] which is a consequence of the absence of the flat edge states at Fermi level.

In [10] we found that the tridiagonal method has an advantage in studying the edge properties effects on the edge localized states due to its ability to separate the edges modes from area modes in case of the 2D square lattice.

Therefore in this work, the tridiagonal method is used to study the effect of edge sites properties on the edge localized states of semi-infinite zigzag 2D honeycomb sheet as study case. The similarity between semi-infinite ZGNR and semi-infinite antiferromagnetic as both two-sublattice structure guide us to follow the tridiagonal method steps used in study the surface modes of Heisenberg antiferromagnetic [11, 12]. The method allow us also to study the effect of impurities introduced substitutionally in impurities localized states of the semi infinite ZGNR.

II. THEORY FOR EDGE STATES AND IMPURITY STATES

The structure of semi-infinite ZGNR is a honeycomb lattice of carbon atoms with two sublattices denoted as A and B. The geometry of a graphene nanoribbon with zigzag edges is shown in Figure 1, where the system is infinite in the x direction and has $2N$ rows of carbon atoms in the y direction. To be considered a ribbon, N is a finite integer but here we will extend the study for

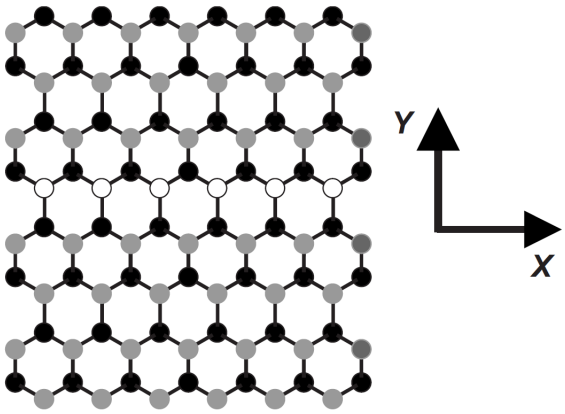

FIG. 1. Geometry of a graphene ribbon with zigzag edges. The black (gray) dots are the sublattice A (B) atoms, where $A(B)$ sublattice type are labeled by index $n(n')$ $(= 1, 2, \cdots, N)$ and the white dots show a row of impurities. Figure taken from [13].

the the semi-infinite case where $N \to \infty$. The $A(B)$ sublattice type lines are labeled with index $n(n')$ where $n(n') = 1, 2, 3, \ldots$. The impurities (which may be silicon or boron, for example) are introduced substitutionally along two different rows of atoms parallel to the x axis. The impurity lines, which preserve the translational symmetry in the x direction, may be any distance apart in the ribbon.

TABLE I. Nearest neighbor hopping matrix elements for the zigzag graphene nanoribbon

Parameter	Zigzag
β	$2t\cos(\sqrt{3}q_x a/2)$
γ	t

Following a microscopic approach in terms of a tight binding model Hamiltonian [8] with neglecting the next nearest neighbor and with follow some recent work for impurities in graphene ribbons [12] the Hamiltonian becomes

$$H = -\sum_{i,j} t_{ij}(a_i^\dagger b_j + a_i b_j^\dagger) \tag{1}$$

where $a_i^\dagger$ (or a_i) creates (or annihilates) an electron on the sublattice A site, and $b_j^\dagger$(or b_j) does the same for the sublattice B site, while t_{ij} is the nearest-neighbor hopping energy between sublattices. In the pure material the hopping energy is denoted by t and its value is known [8] to be ≈ 2.8 eV.

Taking into account the translational symmetry in x direction, a Fourier transform is made to rewrite Equation (1) in a wavenumber representation q_x in the x direction, and the rows are labeled n and n'. The Hamiltonian becomes

$$H = \sum_{q_x,nn'} \left[\tau(q_x) a_{q_x,n} b^{\dagger}_{q_x,n'} + \tau(-q_x) a^{\dagger}_{q_x,n} b_{q_x,n'}\right]. \tag{2}$$

The hopping amplitude factors $\tau_{nn'}(q_x)$ for the zigzag structure have the form

$$\tau_{nn'}(q_x) = t\left[2\cos\left(\frac{\sqrt{3}}{2} q_x a\right)\delta_{n',n} + \delta_{n',n\mp1}\right], \tag{3}$$

or

$$\tau_{nn'}(q_x) = \beta\delta_{n',n} + \gamma\delta_{n',n\mp1}, \tag{4}$$

where the assignment of upper or lower signs depends on the sublattice type sequence for rows n and n' (see Appendix A). The definition of β and γ is given Table I. Now we use the equation of motion $i\hbar dX/dt = [X, H]$ for any operator X for the creation and annihilation operators of each row. Taking $\hbar = 1$ and assuming that the modes have a time dependence like $\exp[-i\omega(q_x)t]$, we obtain $2N$ coupled equations:

$$\begin{aligned} \omega(q_x) a_{q_x,n} &= \sum_{q_x,n'} \tau_{nn'}(-q_x) b_{q_x,n'} \\ \omega(q_x) b_{q_x,n'} &= \sum_{q_x,n} \tau_{n'n}(q_x) a_{q_x,n'}. \end{aligned} \tag{5}$$

Expanding and rearranging the Equations (5) (see Appendix A) such that coupled equations between sublattice A and sublattice B operators, could be written in the following form

$$\begin{aligned} -a_{q_x,n-1} + \frac{\left\{\omega^2(q_x) - \left(\beta^2 + \gamma^2\right)\right\}}{\beta\gamma} a_{q_x,n} - a_{q_x,n+1} &= 0 \\ b_{q_x,n'} - \frac{\gamma}{\omega(q_x)} a_{q_x,n} - \frac{\beta}{\omega(q_x)} a_{q_x,n+1} &= 0 \end{aligned} \tag{6}$$

Equations (6) could be written in the following supermatrix equation [11]

$$\begin{pmatrix} A_N + \Delta A_N & O_N \\ B_N & I_N \end{pmatrix} \begin{pmatrix} a_N \\ b_N \end{pmatrix} = 0, \tag{7}$$

where O_N is the null matrix, I_N the identity matrix, $a_N(b_N)$ operator column vector, and

$$A_N = \begin{pmatrix} \zeta & -1 & 0 & 0 & 0 & \cdots \\ -1 & \zeta & -1 & 0 & 0 & \cdots \\ 0 & -1 & \zeta & -1 & 0 & \cdots \\ 0 & 0 & -1 & \zeta & -1 & \cdots \\ \vdots & \vdots & \vdots & \vdots & \vdots & \ddots \end{pmatrix} \tag{8}$$

and

$$B_N = \begin{pmatrix} \eta & 0 & 0 & 0 & 0 & \cdots \\ \lambda & \eta & 0 & 0 & 0 & \cdots \\ 0 & \lambda & \eta & 0 & 0 & \cdots \\ 0 & 0 & \lambda & \eta & 0 & \cdots \\ \vdots & \vdots & \vdots & \vdots & \vdots & \ddots \end{pmatrix}, \tag{9}$$

the elements of above matrices are defined by

$$\zeta = \frac{\left\{\omega^2(q_x) - \left(\beta^2 + \gamma^2\right)\right\}}{\beta\gamma}, \qquad \eta = \frac{-\gamma}{\omega(q_x)}, \qquad \lambda = \frac{-\beta}{\omega(q_x)}. \tag{10}$$

The edge properties have been separated from the area "bulk" properties of ZGNR by forming the matrix ΔA_N. To simplify the calculations we consider only putting one or two impurities lines in rows numbers n_0 and n_0' of sublattice A such that their properties could be separated form area properties in the same way the edge properties separated before by including them in the matrix ΔA_N. In this case the matrix ΔA_N has the following form

$$\Delta A_N = \begin{pmatrix} \Delta_e & \Delta_s & 0 & 0 & 0 & 0 & 0 & 0 & 0 & 0 & 0 & \cdots \\ \Delta_s & 0 & 0 & 0 & 0 & 0 & 0 & 0 & 0 & 0 & 0 & \cdots \\ 0 & 0 & 0 & 0 & 0 & 0 & 0 & 0 & 0 & 0 & 0 & \cdots \\ 0 & 0 & 0 & 0 & \Delta_{In_0} & 0 & 0 & 0 & 0 & 0 & 0 & \cdots \\ 0 & 0 & 0 & \Delta_{In_0} & \Delta_{n_0} & \Delta_{In_0} & 0 & 0 & 0 & 0 & 0 & \cdots \\ 0 & 0 & 0 & 0 & \Delta_{In_0} & 0 & 0 & 0 & 0 & 0 & 0 & \cdots \\ 0 & 0 & 0 & 0 & 0 & 0 & 0 & 0 & 0 & 0 & 0 & \cdots \\ 0 & 0 & 0 & 0 & 0 & 0 & 0 & 0 & \Delta_{In_0'} & 0 & 0 & \cdots \\ 0 & 0 & 0 & 0 & 0 & 0 & 0 & \Delta_{In_0'} & \Delta_{n_0'} & \Delta_{In_0'} & 0 & \cdots \\ 0 & 0 & 0 & 0 & 0 & 0 & 0 & 0 & \Delta_{In_0'} & 0 & 0 & \cdots \\ 0 & 0 & 0 & 0 & 0 & 0 & 0 & 0 & 0 & 0 & 0 & \cdots \\ \vdots & \vdots & \vdots & \vdots & \vdots & \vdots & \vdots & \vdots & \vdots & \vdots & \vdots & \ddots \end{pmatrix}, \tag{11}$$

the elements of ΔA_N matrix are defined by

$$\begin{aligned}
&\Delta_e = \zeta_e - \zeta, \qquad \Delta_s = \frac{\beta\gamma - \beta_e\tau_e}{\beta\gamma}, \qquad \zeta_e = \frac{\left\{\omega^2(q_x) - \left(\beta_e^2 + \tau_e^2\right)\right\}}{\beta\gamma}, \\
&\Delta_{n_0} = \zeta_{n_0} - \zeta, \qquad \Delta_{In_0} = \frac{\beta\gamma - \beta_I\tau_I}{\beta\gamma}, \qquad \zeta_{n_0} = \frac{\left\{\omega^2(q_x) - \left(\beta_{n_0}^2 + \tau_{n_0}^2\right)\right\}}{\beta\gamma}, \\
&\Delta_{n_0'} = \zeta_{n_0'} - \zeta, \qquad \Delta_{In_0'} = \frac{\beta\gamma - \beta_{In_0'}\tau_{In_0'}}{\beta\gamma}, \qquad \zeta_{n_0'} = \frac{\left\{\omega^2(q_x) - \left(\beta_{n_0'}^2 + \tau_{n_0'}^2\right)\right\}}{\beta\gamma},
\end{aligned} \tag{12}$$

where the edge hopping t_e, the first impurities line hoping t_{n_0}, and the second impurities line hoping $t_{n_0'}$ have replaced the ZGNR interior area sites hoping t in the definition of β and γ in Table I to obtain the edge and impurities counterpart.

Follow the steps of Heisenberg antiferromagnetic case [11] and the algebra of block matrices [14], one define the supermatrix G

$$G = \begin{pmatrix} A_N & O_N \\ B_N & I_N \end{pmatrix}^{-1} = \begin{pmatrix} (A_N)^{-1} & O_N \\ -B_N(A_N)^{-1} & I_N \end{pmatrix}. \tag{13}$$

Multiplying Equation (13) in Equation(7), we get the following

$$\begin{aligned}
(I_N + (A_N)^{-1}\Delta A_N)a_N = 0 \\
(-B_n(A_N)^{-1}\Delta A_N)a_N + b_N = 0
\end{aligned} \tag{14}$$

Define the following matrix

$$D_N = I_N + (A_N)^{-1}\Delta A_N \tag{15}$$

The matrix D_N could be written in the following partition form (see Appendix B)

$$D_N = \left(\begin{array}{c|c} Q & O \\ \hline S & I \end{array}\right), \tag{16}$$

where O is a square null matrix, I a square identity matrix, S a square submatrix of D_N, and Q is square submatrix of D_N with dimension of $n_0' + 1 \times n_0' + 1$.

The elements for the inverse of tridgional matrix A_N [11, 15–18], i.e. the matrix $(A_N)^{-1}$ is given as following:

$$((A_N)^{-1})_{nm} = \frac{x^{n+m} - x^{|n-m|}}{x + x^{-1}}, \tag{17}$$

where x is a complex variable such that $|x| \leq 1$ and $x + x^{-1} = \zeta$. As mentioned in [10], the values of x should satisfy the following boundary and physical conditions [19]. The area modes

are oscillating waves inside the nanoribbon, which requires that x must be imaginary exponential $x = e^{iq_y a/2}$ with $|x| = 1$. From the definition of ζ and x parameters, the dispersion relation for the area band is given by

$$\begin{aligned} \zeta = x + x^{-1} &= e^{iq_y a/2} + e^{-iq_y a/2} = 2\cos(q_y a/2) \\ &= \frac{\left\{\omega_B^2(q_x, q_y) - \left(\beta^2 + \gamma^2\right)\right\}}{\beta\gamma} \\ \omega_B(q_x, q_y) &= \pm t\sqrt{1 + 4\cos^2\left(\frac{\sqrt{3}q_x a}{2}\right) + 4\cos\left(\frac{q_y a}{2}\right)\cos\left(\frac{\sqrt{3}q_x a}{2}\right)} \end{aligned} \tag{18}$$

This expression for the 2D area band for the zigzag nanoribbons is very similar to the extended graphene electronic dispersion relation given in [8]. This expression also shows the same general features of graphene band structure [8].

While the edge modes are localized on the edge and they are decaying exponentially inside the nanoribbon, which requires that x must be real and less than 1 for edge modes. The edge modes are obtained by requiring the determinant of the coefficients for a_n operator column vector to vanish [11, 19, 20]:

$$|D_N| = \det\left[\left(\begin{array}{c|c} Q & O \\ \hline S & I \end{array}\right)\right], \tag{19}$$

using the rules for obtaining the determinant of partitioned matrices [14], Equation (19) become

$$|D_N| = |Q||I - S\,Q^{-1}O| = |Q|, \tag{20}$$

the localized edge and impurities states, i.e. the edge and impurities dispersion relations, for the semi-infinite zigzag are obtained by taking the limit of Equation (20) as $N \to \infty$

$$\lim_{N\to\infty} |D_N| = \lim_{N\to\infty} |Q| = |Q|. \tag{21}$$

In the case of taking only the edge properties effect on the edge localized states, i.e there is no any impurities lines inside the sheet, Equation (21) become

$$\det(Q) = \begin{vmatrix} A_{11}^{-1}\Delta_e + A_{12}^{-1}\Delta_s + 1 & A_{11}^{-1}\Delta_s \\ A_{21}^{-1}\Delta_e + A_{22}^{-1}\Delta_s & A_{21}^{-1}\Delta_s + 1 \end{vmatrix} = 0, \tag{22}$$

which give

$$\Delta_s^2 x^5 - 2\Delta_s x^4 - (2\Delta_s^2 + \Delta_e)x^3 - (1 - 2\Delta_s)x^2 + (\Delta_s^2 + \Delta_e)x - 1 = 0. \tag{23}$$

In case the interaction of the edge with the interior sites is not affected with the edge sites properties, i.e. $\Delta_s = 0$, Equation (21) become

$$\det(A) = \begin{vmatrix} A_{11}^{-1}\Delta_e + 1 & 0 \\ A_{21}^{-1}\Delta_e & 1 \end{vmatrix} = A_{11}^{-1}\Delta_e + 1 = 0 \tag{24}$$

which is the same expression obtained for Heisenberg antiferromagnetic [11].

III. RESULTS

Figures 2 and 3 show the edge localized states of semi-infinite zigzag graphene sheet for different edge hopping to area hopping ratios calculated with $\Delta_s = 0$ using Equation 24 for Figure 2 and calculated with $\Delta_s \neq 0$ using Equation 22 for Figure 3. The Figures show that the dispersion of the edge localized states depends on both the edge sites hopping properties and their effect on the interaction with the interior sites in the zigzag sheet.

The Figures begin with edge hopping equal to zero, which could be done by saturating the carbons atoms on the edge. In this hopping value both calculations (with and without Δ_s) result in an extended flat localized edge state through the whole Brilloin zone at Fermi level $\omega_F/t = 0$. This is due to the localized edge wave functions which agree with density-functional theory (DFT) calculations for finite ribbon [21].

As the edge hopping increases from zero, the dispersion of the edge localized state begin to have a percentage of it laying at Fermi level $\omega_F = 0$, and the remaining percentage liftoff from the Fermi level. The percentage of the edge dispersion that laying at Fermi level is important to the electronic properties of the zigzag edged graphene nanoribbon.

To study the variation of the edge dispersions percentage laying at Fermi level with the changing of the edge hopping and in the same time to easily clarify the data displayed in Figures 2 and 3, we define the following three parameters for each given edge hopping value. The first one is the Relative Localized Density of States near Fermi level (FRLDOS), which is calculated computationally by counting the total number of points in the localized edge dispersion with $\omega/t < 0.2$. The second parameter is the Total Relative Localized Density of States (TRLDOS), which is calculated computationally by counting the total number of points in the localized edge dispersion, which is a relative measure of its total density of states. The third parameter is the difference between FRLDOS and TRLDOS which represent the liftoff percentage of the edge localized state dispersion from Fermi level (LOFRLDOS).

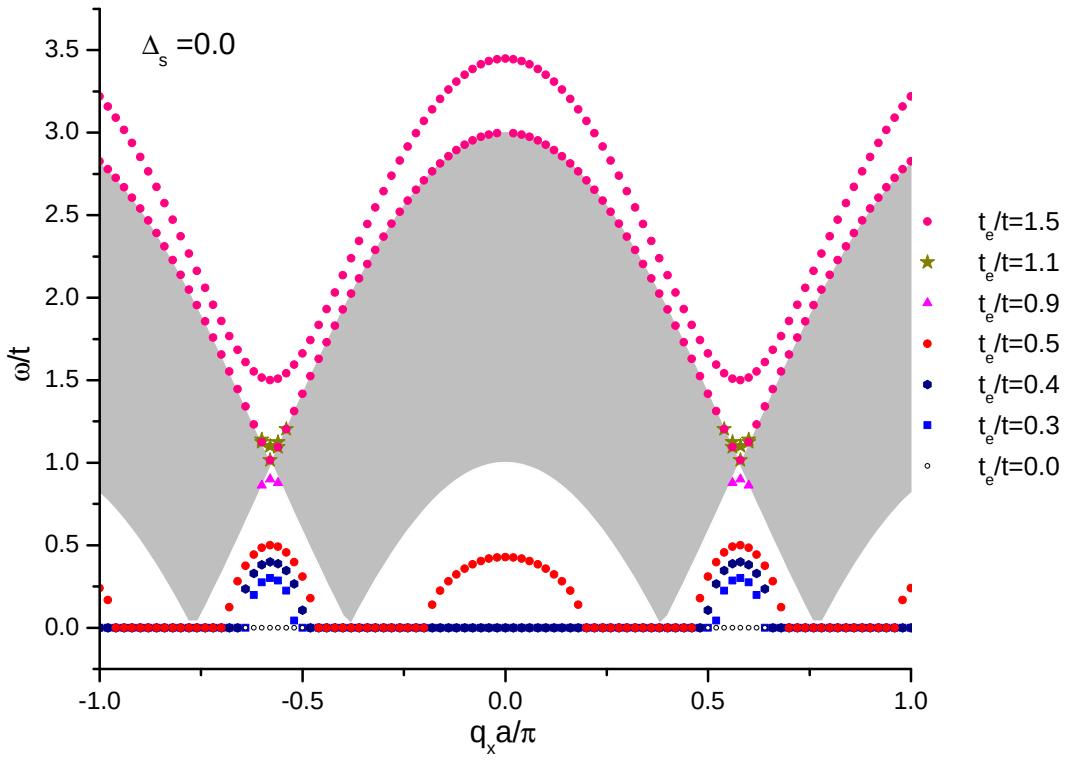

FIG. 2. Edge localized states for edge with different edge hopping calculated with $\Delta_s = 0$, the shaded band represent area modes continuum.

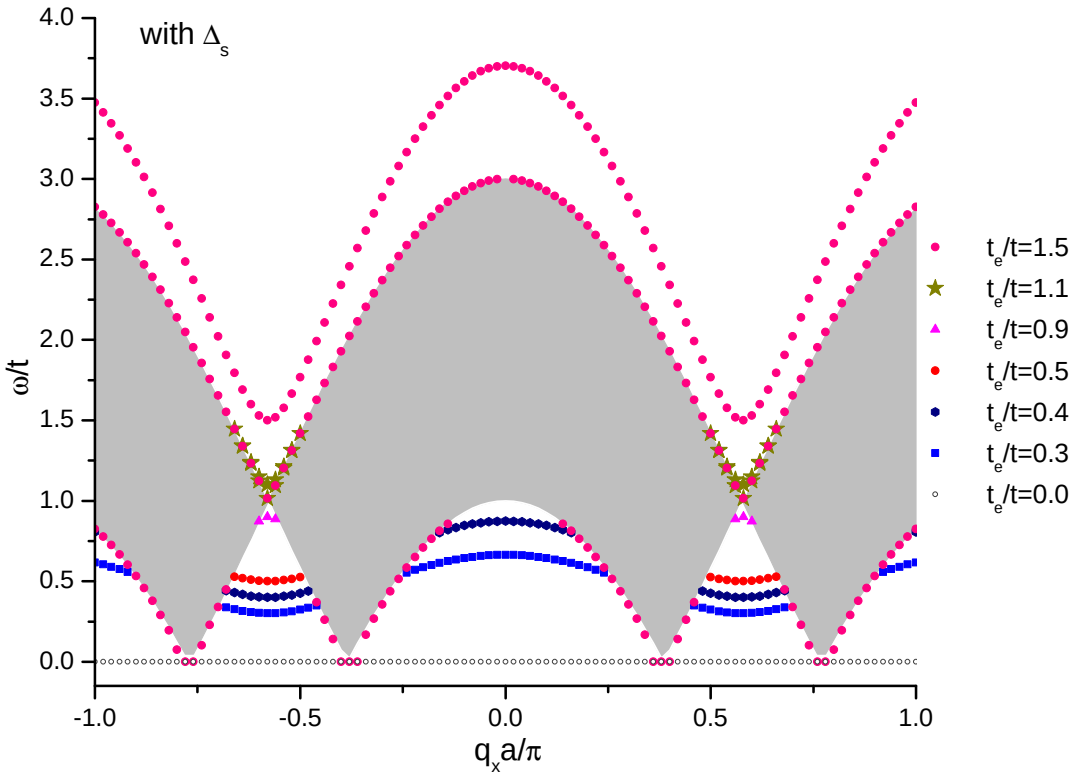

FIG. 3. Edge localized states for edge with different edge hopping calculated with $\Delta_s \neq 0$, the shaded band represent area modes continuum.

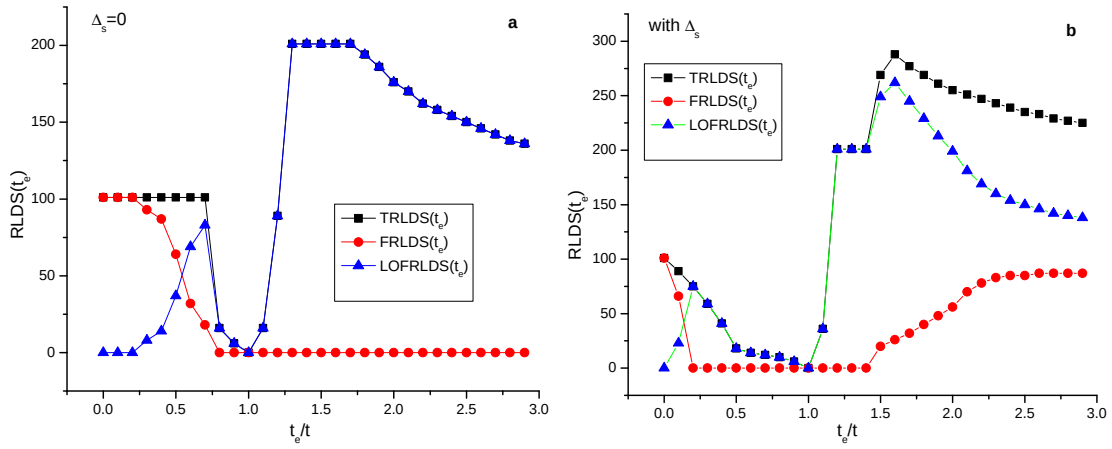

FIG. 4. The variation of TRLDOS, FRLDOS, and LOFRLDOS as a function of edge hopping form 0 to 2.9. (a) for $\Delta_s = 0$ and (b) for $\Delta_s \neq 0$.

Figure 4 shows the variation of TRLDOS, FRLDOS, and LOFRLDOS for edge localized states as a function of edge to area hopping ratio form 0 to 2.9 with increment of 0.1, the (a) sub Figure represent the calculation with $\Delta_s = 0$, while (b) sub Figure represent the calculation with $\Delta_s \neq 0$.

With the help of the comparison between Figure 4(a) and Figure 2 and the comparison between Figure 4(b) and Figure 3, the variation of the edge localized states dispersion with different edge hopping values is described as follow:

First, for the dispersion of localized edge state calculated using $\Delta_s = 0$, starting with edge hopping equal to zero the Figure 4(a) shows that FRLDOS is equal to TRLDOS which means that the edge localized state lays completely in the Fermi level while LOFRLDOS is zero. In Figure 2 it is shown as a flat localized edge state at Fermi level $\omega_F/t = 0$ extended through the whole Brilloin zone as described above. For 2 increment in the edge hopping there is no change in the value of FRLDOS and it is still equal to TRLDOS with LOFRLDOS is equal to zero, which mean that dispersion did not change from as zero hopping. Beginning from edge hopping equal to 0.3 the value of FRLDOS begin to decrease and LOFRLDOS begin to increase while TRLDOS keep constant which means that some of dispersion left off from Fermi level as shown in Figure 2 as a left off near $q_x a/\pi = \pm 0.5$. As edge hopping reach 0.5 the TRLDOS still keep constant while FRLDOS still decreasing and LOFRLDOS still increases which means that more dispersion left off from Fermi level as shown in Figure 2 as increase in the left off near $q_x a/\pi = \pm 0.5$ and around $q_x a/\pi = \pm 0.0$. At edge hopping 0.8 the TRLDOS drop quickly to small value and it is equal to LOFRLDOS while FRLDOS become zero which means that most the edge localized

dispersion disappear which shown in edge hopping 0.9 in Figure 2 as small edge localized points near the intersection of the area band segments. When edge hopping is equal to interior hopping, the edge localized states completely disappear. Figure 4(a) shows that FRLDOS is equal to zero in edge hopping range $0.9 - 2.9$. As the edge hopping increases from 1 to 2.9, LOFRLDOS is equal to TRLDOS. The LOFRLDOS increases very quickly to large value with increasing of edge hopping from 1 to 1.3, and then keep constant in the edge hopping range $1.3 - 1.7$ after that range LOFRLDOS decrease slowly. This behavior is shown in Figure 2 as increasing in the edge localized states above the area band.

In the second case, the dispersion of localized edge state calculated using $\Delta_s \neq 0$, starting with edge hopping equal to zero the Figure 4(b) shows that FRLDOS is equal to TRLDOS which means that the edge localized state lays completely in the Fermi level while LOFRLDOS is zero, in Figure 3 it is shown as a flat localized edge state at Fermi level $\omega_F/t = 0$ extended through the whole Brilloin zone as described above. At the edge hopping equal to 0.1 the values of FRLDOS and TRLDOS begin to decrease and LOFRLDOS begin to increase which means that some of dispersion left off from Fermi level. In the edge hopping range from 0.2 to 1.4, the FRLDOS become zero and TRLDOS become equal to LOFRLDOS. In edge hopping range 0.2 to 1, the LOFRLDOS decreases to a zero value, which is shown in Figure 3 as decreasing in the edge localized states dispersion, and at the same time the edge localized state shifting up in the energy. It is very important to note that at edge hopping 0.5, the edge localized states dispersion become very similar to the famous peculiar edge localized state for graphene zigzag nanoribbon [5–8] but here shifted from Fermi level due to the edge hopping properties. When edge hopping is equal to interior hopping, the edge localized states completely disappear. The LOFRLDOS increases very quickly to large value with increasing of edge hopping from 1 to 1.2, and then remains constant in the edge hopping range $1.2 - 1.4$. After that range, the LOFRLDOS increase to a peak at edge hopping 1.6 and then it begins to slowly decrease until edge hopping 2.9. Starting from the edge hopping 1.4, the LOFRLDOS begins to slowly increase with increasing the edge hopping until the edge hopping reach 2.3, then the LOFRLDOS begins converge to a nearly constant value. While the TRLDOS increase to a peak at edge hopping 1.6 and it then begins to slowly decrease with increasing the edge hopping. The behavior of the three parameters is displayed in Figure 2 as a change in the edge localized states around the area band.

The effects of both the impurities hopping and the impurities line position on the impurities localized states have been calculated using Equation 21 and the results are shown in Figures 5.

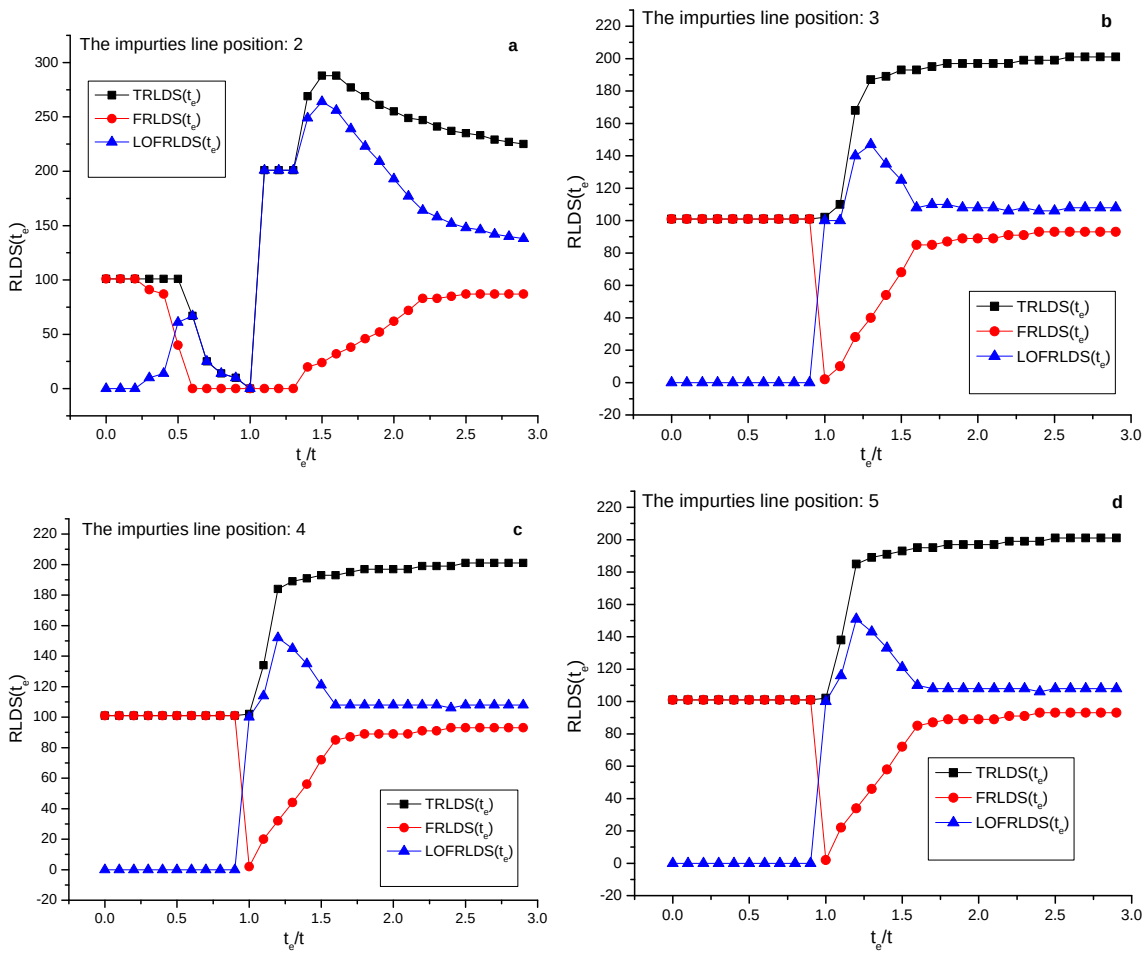

FIG. 5. The variation of TRLDOS, FRLDOS, and LOFRLDOS as a function of impurities hopping form 0 to 2.9 for the impurities line in sublattice *A* at positions (a) 2, (b) 3, (c) 4, (d) 5.

This calculation was done considering the edge hopping is equal to 1.

Figures 5 show the variation of TRLDOS, FRLDOS, and LOFRLDOS as a function of impurities hopping form 0 to 2.9 for the impurities line in sublattice *A* at positions (a) 2, (b) 3, (c) 4, (d)5. It is clear that the dispersion of the impurities localized states for impurities line at second raw of the sublattice *A* is very similar to the dispersion of the edge localized states described above. Beginning from position three in the sublattice *A*, the dispersion of the impurities localized states becomes completely different and nearly independent on the impurities line position in the sublattice *A*.

Figures 5(a), (b), and (c) show that for the impurities hopping range form 0 to 0.9 the FRLDOS is equal to TRLDOS which means that the impurities localized state lays completely in the Fermi level while LOFRLDOS is zero. In Figure 3 it is shown as a flat localized edge state at Fermi

level $\omega_F/t = 0$ extended through the whole Brilloin zone as described above. At the impurities hopping equal to 1 the FRLDOS switches to zero while LOFRLDOS changes to the value that keeps TRLDOS constant. This means that the impurities localized state is completely lay off from Fermi level with keeping its density of states constant. As impurities hopping from 1 to 1.3 the LOFRLDOS rapidly increases to a peak in its value, it then decreases until the impurities hopping reach 1.7 then the LOFRLDOS begin converging to nearly a constant value. Likewise, as impurities hopping from 1 to 1.7 the FRLDOS increase until the impurities hopping reach 1.7 the FRLDOS begin converging to nearly a constant value lower that LOFRLDOS value. While the TRLDOS has fast increases in edge hopping range from 1 to 1.3 and then it begin converging to a nearly high constant value.

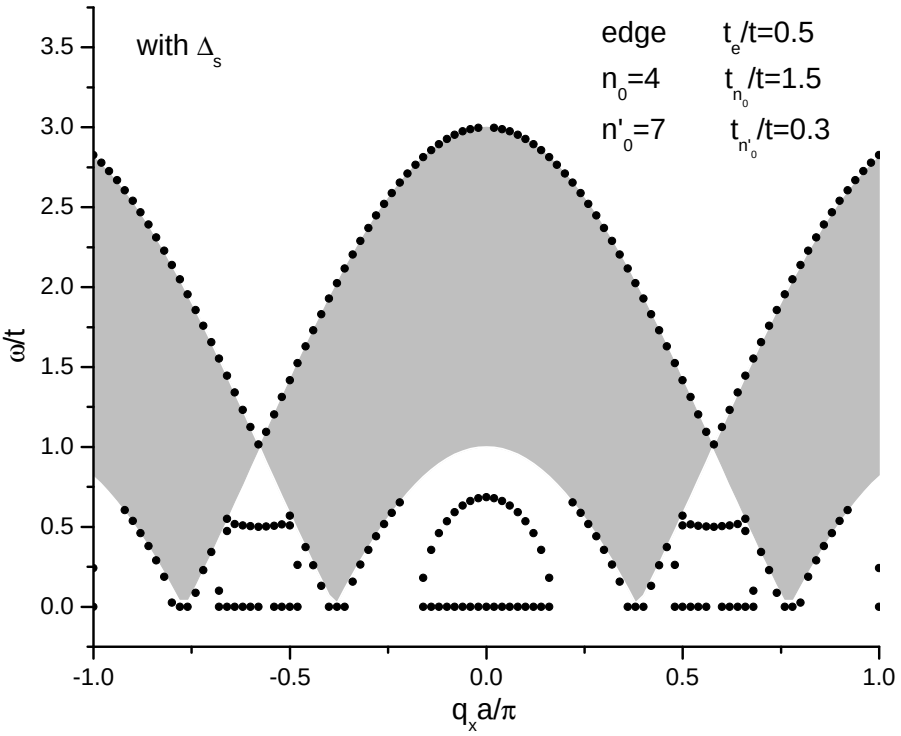

FIG. 6. Edge and impurities localized states the black dots for edge and two lines of impurities at sublattice *A*, the shaded band represent area modes continuum. The Edge hopping is $t_e/t = 0.5$, the first impurities line position is $n_0 = 4$ with impurities hopping $t_{n_0}/t = 1.5$, and the second impurities line position is $n'_0 = 7$ with impurities hopping $t_{n'_0}/t = 0.3$.

IV. DISCUSSION AND CONCLUSIONS

In this work the tridiagonal method was used to study the effect of edge and impurities sites properties on their localized states in semi-infinite zigzag edged 2D honeycomb sheet. It is found that the tridiagonal method calculations provide us with two possibility to study the effect of the edges sites properties on their localized states. In the first one, the interaction of the edge with the interior sites is not affected with the edge sites properties, i.e. $\Delta_s = 0$, and in the second one the interaction of the edge with the interior sites is affected by the edge sites properties, i.e. $\Delta_s \neq 0$.

The results of the case $\Delta_s = 0$ show that the edge localized states dispersion has q_x dependance of the hopping in 1D chain [22] in low edge hopping values, which reflect the completely isolation of edge hopping from interior one. This behavior is away from the expected behavior from tight binding model results and the explanation given in [1].

The results of the case $\Delta_s \neq 0$ show that the edge localized states dispersion has q_x dependance of the hopping in 2D honeycomb but shifted in the energy due to the edge hopping properties and especially at edge hopping 0.5, the edge localized states dispersion become very similar to the famous peculiar edge localized state for graphene zigzag nanoribbon [5–8] but here shifted from Fermi level. which reflect the importance of edge sites properties on the edge hopping with interior sites. In this case the behavior is agree with the expected behavior from tight binding model results and the explanation given in [1].

In case of the effects of both the impurities hopping and the impurities line position on the impurities localized states, the results show that second raw of the sublattice A has very similar edge localized states dispersion, and after that position the impurities localized states become nearly independent on the impurities line position in sublattice A. Also, the results show that introducing impurities in any position of the sheet will produce impurities localized states at Fermi level in all impurities hopping properties, which affecting the electronic properties of the sheet.

The model could be used to study the effects of hopping properties interaction for the edge and the two separated lines of impurities at sublattice A in the edge and the impurities localized states as shown in Figure 6.

The equivalent between the obtained mathematical expressions for edge states in case of zigzag graphene and that obtained for surface spin wave in case of Heisenberg antiferromagnetic [11] reflect their equivalent from geometrical and topological point of view. In the same time it show that result is applicable to the magnetic and the 2D materials have the same geometrical and

topological structure.

Finally, the results of considering the interaction of the edge with the interior sites is affected by the edge sites properties, i.e. $\Delta_s \neq 0$, show a realistic behavior for the dependance of edge localized states of zigzag graphene on the edge sites properties which explaining the experimental results of measured local density of states at the edge of graphene [2], and in the same time removing the inconsistence between the semiconductor behavior found in the experimental data for fabricated GNRs [3, 4] and the expected theoretical semi-metallic behavior calculated without considering the edge properties effect on the edge localized states [5–8].

ACKNOWLEDGMENTS

This research has been supported by the Egyptian Ministry of Higher Education and Scientific Research (MZA).

---

[1] M. Z. Ahmed, *Study of electronic and magnetic excitations in the 2D materials represented by graphene and magnetic nano-ribbons*, Ph.D. thesis, The University of Western Ontario (2011), download pdf version and a Viedo on Sciencestage.com.

[2] Z. Klusek, W. Kozlowski, Z. Waqar, S. Datta, J. Burnell-Gray, I. Makarenko, N. Gall, E. Rutkov, A. Tontegode, and A. Titkov, Applied Surface Science **252**, 1221 (2005).

[3] X. Wang, Y. Ouyang, X. Li, H. Wang, J. Guo, and H. Dai, Phys. Rev. Lett. **100**, 206803 (2008).

[4] Z.-y. L. Bing Huang, Qi-min Yan and W. hui Duan, Frontiers of Physics in China **4**, 269 (2009).

[5] K. Nakada, M. Fujita, G. Dresselhaus, and M. S. Dresselhaus, Phys. Rev. B **54**, 17954 (1996).

[6] K. Wakabayashi, M. Fujita, H. Ajiki, and M. Sigrist, Phys. Rev. B **59**, 8271 (1999).

[7] M. Fujita, K. Wakabayashi, K. Nakada, and K. Kusakabe, Journal of the Physical Society of Japan **65**, 1920 (1996).

[8] A. H. Castro Neto, F. Guinea, N. M. R. Peres, K. S. Novoselov, and A. K. Geim, Rev. Mod. Phys. **81**, 109 (2009).

[9] X. Jia, J. Campos-Delgado, M. Terrones, V. Meunier, and M. S. Dresselhaus, Nanoscale **3**, 86 (2011).

[10] M. Ahmed, (2011), arXiv:1110.4369v1 [cond-mat.mes-hall].

[11] R. E. De Wames and T. Wolfram, Phys. Rev. **185**, 752 (1969).

[12] R. N. C. Filho, U. M. S. Costa, and M. G. Cottam, J. Magn. Magn. Mater. **213**, 195 (2000).

[13] R. N. Costa Filho, G. A. Farias, and F. M. Peeters, Phys. Rev. B **76**, 193409 (2007).

[14] J. R. M. Karim M. Abadir, *Matrix algebra*, Vol. 1 (Cambridge University Press, 2005).

[15] R. N. C. Filho, U. M. S. Costa, and M. G. Cottam, Journal of Magnetism and Magnetic Materials **213**, 195 (2000).

[16] M. G. Cottam and D. E. Kontos, Journal of Physics C: Solid State Physics **13**, 2945 (1980).

[17] M. G. Cottam, Journal of Physics C: Solid State Physics **9**, 2121 (1976).

[18] R. E. De Wames and T. Wolfram, Phys. Rev. **185**, 720 (1969).

[19] M. Cottam and D. Tilley, *Introduction to Surface and Superlattice Excitations*, 2nd ed. (IOP Publishing, 2004).

[20] P. R. L. Heron, *Theory of spin waves in Heisenberg ferromagnetic and antiferromagnetic thin films with nonuniaxial single-ion anisotropy*, Thesis (ph.d.), Faculty of Graduate Studies, University of Western Ontario, London, Ont. (1995).

[21] B. Xu, J. Yin, Y. D. Xia, X. G. Wan, K. Jiang, and Z. G. Liu, Applied Physics Letters **96**, 163102 (2010).

[22] A. Altland and B. Simons, *Condensed matter field theory*, 2nd ed. (Cambridge University Press, 2010).

Appendix A: Rearranging Equations (5)

In this appendix we list the rearrange steps of Equations (5) to obtain Equations (6).

$$\omega(q_x)a_{q_x,n} = \sum_{q_x,n'} \tau_{nn'}(-q_x)b_{q_x,n'}$$
$$\omega(q_x)b_{q_x,n'} = \sum_{q_x,n} \tau_{n'n}(q_x)a_{q_x,n'}.$$

Expanding Equations (5) using the sublattice indexes n and n'

$$\begin{aligned}
\omega(q_x)a_{q_x,1} &= \beta b_{q_x,1} \\
\omega(q_x)a_{q_x,2} &= \gamma b_{q_x,1} + \beta b_{q_x,2} \\
\omega(q_x)a_{q_x,3} &= \gamma b_{q_x,2} + \beta b_{q_x,3} \\
&\vdots \\
\omega(q_x)a_{q_x,n} &= \gamma b_{q_x,n'-1} + \beta b_{q_x,n'}
\end{aligned}$$

$$\begin{aligned}
\omega(q_x)b_{q_x,1} &= \beta a_{q_x,1} + \gamma a_{q_x,2} \\
\omega(q_x)b_{q_x,2} &= \beta a_{q_x,2} + \gamma a_{q_x,3} \\
\omega(q_x)b_{q_x,3} &= \beta a_{q_x,3} + \gamma a_{q_x,4} \\
&\vdots \\
\omega(q_x)b_{q_x,n'} &= \beta a_{q_x,n} + \gamma a_{q_x,n+1}
\end{aligned}$$

divide by $\omega(q_x)$, and rearrange we get

$$b_{q_x,n'} - \frac{\gamma}{\omega(q_x)}a_{q_x,n} - \frac{\beta}{\omega(q_x)}a_{q_x,n+1} = 0$$

$$\omega(q_x)b_{q_x,n'} = \beta a_{q_x,n} + \gamma a_{q_x,n+1}$$

$$\omega(q_x)b_{q_x,n'-1} = \beta a_{q_x,n-1} + \gamma a_{q_x,n}$$

$$\omega(q_x)a_{q_x,n} = \gamma b_{q_x,n'-1} + \beta b_{q_x,n'}$$

$$\omega(q_x)a_{q_x,n} = \gamma\frac{\beta a_{q_x,n-1} + \gamma a_{q_x,n}}{\omega(q_x)} + \beta\frac{\beta a_{q_x,n} + \gamma a_{q_x,n+1}}{\omega(q_x)}$$

$$\omega^2(q_x)a_{q_x,n} = \gamma(\beta a_{q_x,n-1} + \gamma a_{q_x,n}) + \beta(\beta a_{q_x,n} + \gamma a_{q_x,n+1})$$

lead to

$$-a_{q_x,n-1} + \frac{\omega^2(q_x) - (\beta^2+\gamma^2)}{\gamma\beta} a_{q_x,n} - a_{q_x,n+1} = 0$$

Appendix B: The partition of D_N matrix

In this appendix we list the steps of partitioning the D_N matrix.

$$A^{-1} = \begin{pmatrix}
A^{-1}_{11} & A^{-1}_{12} & A^{-1}_{13} & \cdots & A^{-1}_{1n_0-1} & A^{-1}_{1n_0} & A^{-1}_{1n_0+1} & \cdots & A^{-1}_{1n'_0-1} & A^{-1}_{1n'_0} & A^{-1}_{1n'_0+1} & \cdots \\
A^{-1}_{21} & A^{-1}_{22} & A^{-1}_{23} & \cdots & A^{-1}_{2n_0-1} & A^{-1}_{2n_0} & A^{-1}_{2n_0+1} & \cdots & A^{-1}_{2n'_0-1} & A^{-1}_{2n'_0} & A^{-1}_{2n'_0+1} & \cdots \\
A^{-1}_{31} & A^{-1}_{32} & A^{-1}_{33} & \cdots & A^{-1}_{3n_0-1} & A^{-1}_{3n_0} & A^{-1}_{3n_0+1} & \cdots & A^{-1}_{3n'_0-1} & A^{-1}_{3n'_0} & A^{-1}_{3n'_0+1} & \cdots \\
\vdots & \vdots & \vdots & \vdots & \vdots & \vdots & \vdots & \vdots & \vdots & \vdots & \vdots & \cdots \\
A^{-1}_{n1} & A^{-1}_{n2} & A^{-1}_{n3} & \cdots & A^{-1}_{nn_0-1} & A^{-1}_{nn_0} & A^{-1}_{nn_0+1} & \cdots & A^{-1}_{nn'_0-1} & A^{-1}_{nn'_0} & A^{-1}_{nn'_0+1} & \cdots \\
\vdots & \vdots & \vdots & \vdots & \vdots & \vdots & \vdots & \vdots & \vdots & \vdots & \vdots & \cdots \\
A^{-1}_{n'_01} & A^{-1}_{n'_02} & A^{-1}_{n'_03} & \cdots & A^{-1}_{n'_0n_0-1} & A^{-1}_{n'_0n_0} & A^{-1}_{n'_0n_0+1} & \cdots & A^{-1}_{n'_0n'_0-1} & A^{-1}_{n'_0n'_0} & A^{-1}_{n'_0n'_0+1} & \cdots \\
\vdots & \vdots & \vdots & \vdots & \vdots & \vdots & \vdots & \vdots & \vdots & \vdots & \vdots & \ddots
\end{pmatrix} \tag{B1}$$

which is of dimension $N \times N$.

$$\Delta A_N = \begin{pmatrix}
\Delta_e & \Delta_s & 0 & 0 & 0 & 0 & 0 & 0 & 0 & 0 & 0 & \cdots \\
\Delta_s & 0 & 0 & 0 & 0 & 0 & 0 & 0 & 0 & 0 & 0 & \cdots \\
0 & 0 & 0 & 0 & 0 & 0 & 0 & 0 & 0 & 0 & 0 & \cdots \\
0 & 0 & 0 & 0 & \Delta_{In_0} & 0 & 0 & 0 & 0 & 0 & 0 & \cdots \\
0 & 0 & 0 & \Delta_{In_0} & \Delta_{n_0} & \Delta_{In_0} & 0 & 0 & 0 & 0 & 0 & \cdots \\
0 & 0 & 0 & 0 & \Delta_{In_0} & 0 & 0 & 0 & 0 & 0 & 0 & \cdots \\
0 & 0 & 0 & 0 & 0 & 0 & 0 & 0 & 0 & 0 & 0 & \cdots \\
0 & 0 & 0 & 0 & 0 & 0 & 0 & 0 & \Delta_{In'_0} & 0 & 0 & \cdots \\
0 & 0 & 0 & 0 & 0 & 0 & 0 & \Delta_{In'_0} & \Delta_{n'_0} & \Delta_{In'_0} & 0 & \cdots \\
0 & 0 & 0 & 0 & 0 & 0 & 0 & 0 & \Delta_{In'_0} & 0 & 0 & \cdots \\
0 & 0 & 0 & 0 & 0 & 0 & 0 & 0 & 0 & 0 & 0 & \cdots \\
\vdots & \vdots & \vdots & \vdots & \vdots & \vdots & \vdots & \vdots & \vdots & \vdots & \vdots & \ddots
\end{pmatrix}, \tag{B2}$$

which is of dimension $N \times N$.

$$D_N = I_N + (A_N)^{-1}\Delta A_N \tag{B3}$$

therefore the D_N dimension is $N \times N$ with the following elements:

$$\begin{aligned}
D_{i1} &= A_{i1}^{-1}\Delta_e + A_{i2}^{-1}\Delta_s + \delta_{i1} \\
D_{i2} &= A_{i1}^{-1}\Delta_s + \delta_{i2} \\
D_{in_0-1} &= A_{in_0}^{-1}\Delta_{In_0} + \delta_{in_0-1} \\
D_{in_0} &= A_{in_0-1}^{-1}\Delta_{In_0} + A_{in_0}^{-1}\Delta_{n_0} + A_{in_0+1}^{-1}\Delta_{In_0} + \delta_{in_0} \\
D_{in_0+1} &= A_{in_0}^{-1}\Delta_{In_0} + \delta_{in_0+1} \\
D_{in_0'-1} &= A_{in_0'}^{-1}\Delta_{In_0'} + \delta_{in_0'-1} \\
D_{in_0'} &= A_{in_0'-1}^{-1}\Delta_{In_0'} + A_{in_0'}^{-1}\Delta_{n_0'} + A_{in_0'+1}^{-1}\Delta_{In_0'} + \delta_{in_0'} \\
D_{in_0'+1} &= A_{in_0'}^{-1}\Delta_{In_0'} + \delta_{in_0'+1} \\
D_{ij} &= \delta_{ij} \text{ if both } j \text{ and } i \text{ are not equal to either } n \text{ or } m
\end{aligned}$$

$$D_N = \begin{pmatrix}
D_{11} & D_{12} & D_{13} & \cdots & D_{1n_0-1} & D_{1n_0} & D_{1n_0+1} & \cdots & D_{1n_0'-1} & D_{1n_0'} & D_{1n_0'+1} & \cdots \\
D_{21} & D_{22} & D_{23} & \cdots & D_{2n_0-1} & D_{2n_0} & D_{2n_0+1} & \cdots & D_{2n_0'-1} & D_{2n_0'} & D_{2n_0'+1} & \cdots \\
D_{31} & D_{32} & D_{33} & \cdots & D_{3n_0-1} & D_{3n_0} & D_{3n_0+1} & \cdots & D_{3n_0'-1} & D_{3n_0'} & D_{3n_0'+1} & \cdots \\
\vdots & \vdots & \vdots & \vdots & \vdots & \vdots & \vdots & \vdots & \vdots & \vdots & \vdots & \cdots \\
D_{n_01} & D_{n_02} & D_{n_03} & \cdots & D_{n_0n_0-1} & D_{n_0n_0} & D_{n_0n_0+1} & \cdots & D_{n_0n_0'-1} & D_{n_0n_0'} & D_{n_0n_0'+1} & \cdots \\
\vdots & \vdots & \vdots & \vdots & \vdots & \vdots & \vdots & \vdots & \vdots & \vdots & \vdots & \cdots \\
D_{n_0'1} & D_{n_0'2} & D_{n_0'3} & \cdots & D_{n_0'n_0-1} & D_{n_0'n_0} & D_{n_0'n_0+1} & \cdots & D_{n_0'n_0'-1} & D_{n_0'n_0'} & D_{n_0'n_0'+1} & \cdots \\
\vdots & \vdots & \vdots & \vdots & \vdots & \vdots & \vdots & \vdots & \vdots & \vdots & \vdots & \ddots
\end{pmatrix}$$

which give the following partition of D_N matrix

$$D_N = \left(\begin{array}{c|c} Q & O \\ \hline S & I \end{array}\right), \tag{B4}$$

where O is a square null matrix, I a square identity matrix, S a square submatrix of D_N, and Q is square submatrix of D_N with dimension of $n_0' + 1 \times n_0' + 1$.